

Optimize Your Process



Use Optimal Vacuum Solutions to Implement Renewable Energy

Your added value

- Pumps for vacuum generation down to ultra-high vacuum
- Vacuum measurement and analysis equipment
- Leak detectors and integrity test systems
- Chambers, components and valves
- Pumping stations and customized solutions

Metal Chalcogenides: Next Generation Photovoltaic Materials?

Francisco Palazon

Metal chalcogenides have recently been highlighted as so-far overlooked semiconductors that could play an important role in the future of photovoltaics (PV). Indeed, the blooming field of emergent PV technologies is still in search for stable, efficient, and environmentally-friendly light-harvesting materials to be used either in single-junction solar cells or multijunction devices in combination with silicon or another absorbers. Under the broad terms of metal chalcogenides, there exists a plethora of semiconductor materials with different chemical, structural, and optoelectronic characteristics. While some have already been implemented in solar cells with power conversion efficiencies up to 4–5%, others are only theoretically described. This perspective article offers a general overview of these materials as potential next-generation absorbers in PV and also discusses possible limitations, not only related to intrinsic materials' properties but also to processing conditions.

Among the different alternatives to silicon proposed since the 1970s the most promising ones in terms of efficiency are either organic semiconductors or inorganic metal chalcogenides and hybrid organic–inorganic lead halide perovskites. Organic PV, despite a recent jump in efficiency and the development of non-fullerene acceptors, still suffers mainly from insufficient stability.^[4] Inorganic metal chalcogenides and lead halide perovskites, as well as gallium arsenide present different bottlenecks, especially linked to scarcity and/or toxicity of the different elements involved such as cadmium and lead. Furthermore, lead halide perovskites, especially hybrid organic–inorganic ones, suffer from relatively poor stability toward humidity and heat.^[5] Kesterites


($\text{Cu}_2\text{ZnSn}(\text{S:Se})_4$ or CZTS), with a slower evolution in record efficiency than perovskites, could perhaps become a viable alternative based on abundant and low-toxicity elements.^[6] However, the fabrication of high-quality kesterite thin films for PV remains challenging and not easily upscalable. Tin-based perovskites hold some promise to combine the advantages of lead halide perovskites in terms of efficiency, bandgap tunability, and ease of production with a lower toxicity derived from the removal of lead cations. However, to date it is not yet clear if fully replacing lead by tin in metal halide perovskites can result in a stable and viable photovoltaic absorber. Indeed, the instability of Sn(II)-based perovskites represents a major hurdle, with Sn(II) being preferentially oxidized in air to Sn(IV).^[7] This has triggered the research on other lead-free perovskite-inspired materials^[8] including but not limited to vacancy-ordered perovskites such as Cs_2SnI_6 or $\text{Cs}_3\text{Bi}_2\text{Br}_9$. Hence, it is fair to say that the search for alternative light-harvesting materials is still, or perhaps more-than-ever, a timely topic and an exciting research field.^[9]

In this perspective article, we will explore a class of rather overlooked inorganic semiconductors that may play an important role in the future development of photovoltaics: metal chalcogenides. These materials can be very broadly defined as $\text{M}_a\text{X}_b\text{Y}_c$ compounds, where M is one or a combination of several metal cations and X and Y are one or a combination of several chalcogen and halogen anions (a, b, and c can take different values). This broad definition encompasses different materials which can be classified by the nature of the metal cation(s). Several recent review and perspective articles have highlighted the relevance of some of these materials for photovoltaics and related applications.^[10–14] Nevertheless, these are almost exclusively

1. Introduction

The development of photovoltaics (PV) is strongly related to the discovery and implementation of different light-harvesting semiconductor materials.^[1] First generation solar cells were, and still are, based on crystalline silicon. However, despite the predominance of silicon in PV for the last 40 years, alternative absorbers have been investigated either to outperform silicon in specific aspects (e.g., efficiency, ease of production, lightness, or flexibility) or to be used in combination with it in multijunction solar cells. Indeed, recent developments clearly point toward the use of tandem or multijunction devices to reach high power conversion efficiencies (PCEs), beyond the thermodynamic limit for a single-junction device ($\approx 33\%$).^[2] This requires the use of materials with different bandgaps to efficiently harvest different parts of the solar spectrum.^[3]

F. Palazon
Instituto de Ciencia Molecular
ICMol
Universidad de Valencia
46980 Paterna, Spain
E-mail: francisco.palazon@uv.es

 The ORCID identification number(s) for the author(s) of this article can be found under <https://doi.org/10.1002/solr.202100829>.

© 2021 The Authors. Solar RRL published by Wiley-VCH GmbH. This is an open access article under the terms of the Creative Commons Attribution-NonCommercial License, which permits use, distribution and reproduction in any medium, provided the original work is properly cited and is not used for commercial purposes.

DOI: 10.1002/solr.202100829

focused on pnictogen chalcogenides, which are of obvious relevance (see Section 3) but not the only existing candidates. In this section, we will survey some of the most relevant metal chalcogenide materials for photovoltaics with a focus (though not exclusively) on low-toxicity and earth-abundant elements. We will also report and discuss the few existing photovoltaic devices and performances based on these light absorbers. Finally, we will give an outlook to the potential future development of metal chalcogenides as next-generation PV materials.

2. Transition and Post-Transition Metal Chalcogenides (M = Ag, Cu, Sn, Pb, or Others)

Several transition and post-transition metal chalcogenides with different stoichiometries have been experimentally and/or theoretically described, some of which may be judged relevant for PV. Among these, different environmentally-friendly silver-based chalcogenides have been reported. Ag_3SI and Ag_3SBr were first reported by Reuter and Hardel in 1960, who described their antiperovskite crystal structure.^[15] Indeed, this crystal structure is similar to the well-known perovskite structure with cations in place of anions and vice versa (see **Figure 1**). This analogy may be better understood by writing these chalcogenides as ISAg_3 and BrSAg_3 , though the former writing is more common and will be employed hereafter.

Ag_3SI and Ag_3SBr have been studied mainly for use as solid electrolytes owing to their superionic conductivity which was noted already in 1966 by Takahashi and Yamamoto.^[16] This property however varies with the crystalline phase. Indeed at least four different polymorphs exist for Ag_3SI for which only the high-temperature phase may be superionic (ionic conductivity around 1.5 S cm^{-1}) while the two reported stable phases at room

temperature show ionic conductivities one or two orders of magnitude lower.^[17] The discussion on ionic conductivity here is particularly related to seminal claims of ion mobility as a cause for hysteresis in lead halide perovskite-based PV. Indeed, lead halide perovskites have also been reported to be fast ion conductors.^[18] Nevertheless, most publications on perovskite PV of the last few years do not show hysteresis in current–voltage curves. Moreover, Calado et al.^[19] showed that hysteresis in perovskite PV is not directly linked to ion mobility, but rather to poor interfaces with contact layers, which can be suppressed by proper passivation. Hence, high ionic conductivity should not be a barrier for the implementation of Ag_3SX ($X = \text{Br}$ or I) antiperovskites in photovoltaics. Indeed, these antiperovskites appear as relevant alternative materials, especially due to their bandgap around 0.9–1.1 eV at room temperature.^[20,21] This makes them interesting for single-junction solar cells as well as for low-bandgap bottom cells in tandem configurations, although no reports exist to date on these uses. The lack of reports on Ag_3SI - or Ag_3SBr -based PV devices may be in great part simply linked to these materials being overlooked among the many so-called emerging PV materials. However, it may also be due to difficult and energy- and time-consuming synthetic approaches.^[22,23] We should note that Ag_3SI ultrathin films have been produced by laser ablation.^[24] Nevertheless, the target material for laser ablation had to be pre-synthesized in vacuum at 750°C for 3 h, which may be considered as a process that is not promising in terms of upscaling. The development of silver chalcogenide antiperovskite PV appears thus to be limited, at the current moment, by costly synthetic and deposition processes. Notwithstanding this limitation, silver chalcogenide antiperovskites appear promising not only for their environmentally-friendly character and suitable bandgap, but also for their chemical versatility. Indeed, similar to lead halide perovskites, different partial cation- or anion-replacements have been reported including Cu^+ and Cd^+ for Ag^+ or I^- and Cl^- for Br^- in Ag_3SBr .^[25–28] These substitutions lead to changes in conductivity and phase stability. It is foreseeable that bandgap tuning, which was not investigated in these reports, may also be achieved in such mixed-cation and/or mixed-halide antiperovskites. Eventually, Ag_3SBr has also been studied for thermoelectric power generation,^[29] which is a closely related field to photovoltaics.

Aside from silver chalcogenides, other ternary metal sulfides and sulfofluorides may be relevant for photovoltaics. Indeed, $\text{Sn}_5\text{S}_4\text{Cl}_2$, $\text{Cd}_5\text{S}_4\text{Cl}_2$, Sn_4SF_6 , and Cd_4SF_6 were theoretically predicted to be stable compositions with bandgaps throughout the visible range.^[30] Also, $\text{Sn}_5\text{S}_4\text{Cl}_2$ is predicted to have low and balanced electron and hole effective masses of $0.5 m_e$ and $0.4 m_e$. Thus, with a bandgap of 0.9 eV, low charge carrier effective masses and comprising generally low-toxicity elements, this material may be especially suited as low-bandgap absorber in multijunction solar cells.

Lead chalcogenides have also been recently studied and experimentally demonstrated as colloidal nanostructures with kinetically trapped metastable phases at ambient conditions.^[31] In particular, lead sulfohalides are demonstrated with tunable bandgap depending on stoichiometry and halide. $\text{Pb}_4\text{S}_3\text{Br}_2$ nanocrystals have been effectively implemented in single-junction solar cells with an average PCE of 0.2% (see **Figure 2**).

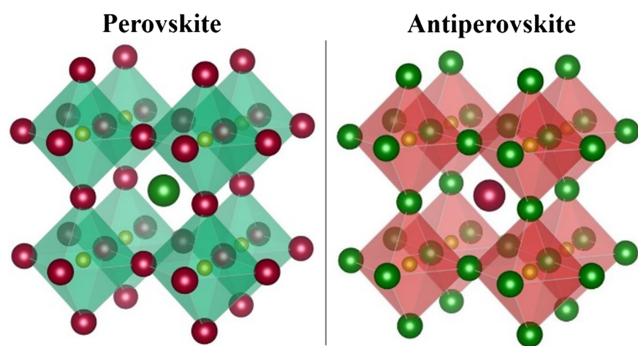


Figure 1. Schematic representation of the perovskite and antiperovskite crystal structure. Both are isostructural but with anions in place of cations and vice versa. The perovskite structure to the left may be obtained for example with green ball = Cs^+ , yellow ball = Pb^{2+} , and red ball = Cl^- (CsPbCl_3). In contrast, the antiperovskite structure may be obtained with red ball = I^- , yellow ball = S^{2-} , and green ball = Ag^+ (Ag_3SI or ISAg_3) for instance. Note that high-symmetry cubic (anti)perovskites are depicted here (based on VESTA rendering of SrTiO_3 crystallographic information file retrieved from the Inorganic Crystal Structure Database). However, slight distortions lead to tetragonal and orthorhombic (anti)perovskites, often more stable at room temperature. More details on different perovskites, antiperovskites, and related structures may be found elsewhere.^[67]

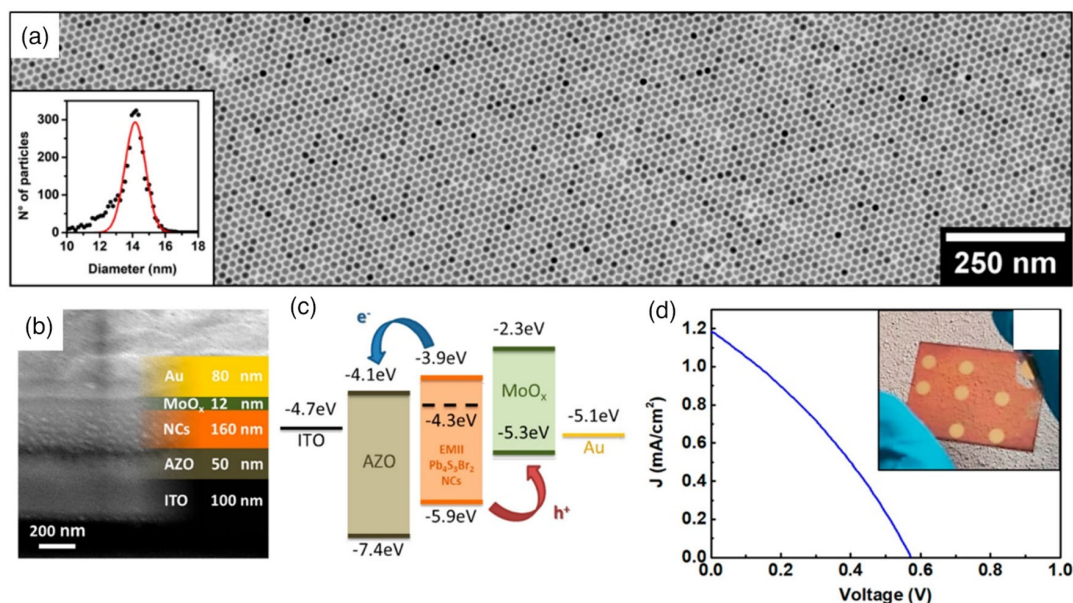


Figure 2. $\text{Pb}_4\text{S}_3\text{Br}_2$ colloidal nanocrystals implemented in a single-junction solar cell. a) Transmission electron microscopy image of the nanocrystals with size distribution inset. b) Cross-section scanning electron microscopy image of the solar cell with legend and c) flat band energy diagram. d) Current density–voltage characteristic and photograph of a representative sample as inset. Adapted with permission.^[31] Copyright 2020, American Chemical Society.

Finally, it might be worth noting that thallium chalcogenide semiconductors such as Tl_6SeI_4 have also been employed for X-ray and gamma-ray detections,^[32] although they are unlikely to be adopted for PV, given the high toxicity of thallium.

3. Heavy Pnictogen Chalcogenides (M = Sb or Bi)

Pnictogen chalcogenides combine a trivalent heavy pnictogen cation and a divalent chalcogenide and monovalent halide anions. They can thus be written with the general chemical formula MXY where $\text{M} = \text{Bi}$ or Sb ; $\text{X} = \text{S}$, Se , or Te ; and $\text{Y} = \text{Cl}$, Br , or I . While they may be viewed as post-transition metal chalcogenides, their particularities and specific relevance for PV as will be discussed hereafter, makes it more convenient to discuss them in a separate section. Heavy pnictogen chalcogenides are also commonly referred to as V-VI-VII materials, following the widespread notation of inorganic semiconductors, based on the element groups in the periodic table. Similar to what can be said about lead halide perovskites,^[33] V-VI-VII semiconductors cannot be considered *new* materials. Indeed, the synthesis of antimony sulfide, SbSI , can be traced back to Henry and Garot in 1824.^[34] In the 1960s these materials started to gain more interest in the scientific community, due to their optical and electrical properties. Especially, photoconductivity and ferroelectricity of antimony sulfide were demonstrated by Nitsche, Merz, and coworkers in 1960 and 1962.^[35,36] Moreover, Nitsche and Merz experimentally revealed in 1960 the distinct colors of the different V-VI-VII semiconductors, which can be related to their bandgap tunability (see **Table 1**). This is possibly the main characteristic sought after today for the development of multijunction photovoltaic devices.

Table 1. Table adapted from Nitsche and Merz.^[35] λ_{max} indicates the wavelength of maximum photocurrent.

Material	Color	λ_{max}
SbSBr	Orange needles	5450–5500 Å
SbSI	Red needles	6300–6400 Å
SbSeBr	Dark red needles	6500 Å
SbSeI	Black needles	6500 Å
SbTeI	Black needles	7200 Å
BiSBr	Dark red needles	6350 Å
BiSI	Black needles	7850 Å
BiSeCl	Dark red needles	High dark current
BiSeBr	Black needles	High dark current
BiSeI	Black needles	High dark current

Table 1 also reveals a needle shape for all V-VI-VII crystals. This may be linked to the pseudo-1D crystal structure of these materials (**Figure 3**)^[37] and growth rate anisotropy, which can be problematic for the formation of dense thin films in a planar photovoltaic device.^[38]

Following the reports on photoconductive,^[35] electro-optical,^[39] electro-mechanical,^[39] and ferroelectric^[36] effects from 1960 to 1962, SbSI has been investigated for different electronic applications. In particular, in the last two decades, several demonstrations have been published on the implementation of SbSI in different devices. In 2002 Surthi et al.^[40] grew thin films of SbSI by pulsed-laser deposition and used them for ferroelectric memory applications. More recently, in 2015

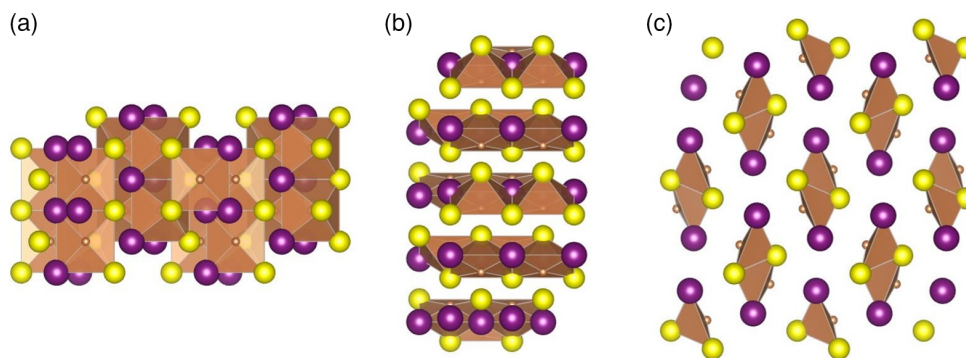


Figure 3. SbSI crystal structure viewed along the a, b, and c axes. Yellow balls represent S^{2-} , purple balls represent I^- and orange balls represent Sb^{3+} . The view along the c-axis highlights the 1D structure that can be related to the macroscopic needle morphology (see Table 1). Figure created with VESTA software based on crystallographic information file 25572 from the Inorganic Crystal Structure Database.

Chen et al.^[41] used SbSI single crystals as photodetectors while in 2017 SbSI nanowires were used in combination with carbon nanotubes for photocatalysis by Tasviri and Sajavi-Hezave.^[42] These results suggest that SbSI and other V-VI-VII semiconductors may also be of interest for photovoltaic applications. In fact, theoretical calculations by Walsh, Scanlon, and coworkers in 2015–2017 pointed out the relevance of these materials which had “so far been passed over for other materials” in PV.^[37,43,44] Similarly, Wlázlak et al. stressed the relevance of these “rediscovered semiconductors” in a review article from 2018.^[10] In particular, the authors highlight several features of these materials that can also be found in lead halide perovskites and have contributed to the success of the latter in this field, including low electron and hole effective masses, photoferroicity, and the ns^2 configuration of trivalent heavy pnictogens (*idem* to Pb(II)) which is considered to be the origin to the defect tolerance of lead halide perovskites.

To the best of our knowledge, the first experimental use of V-VI-VII semiconductors as light-harvesting materials in solar cells was reported by Nie et al. in 2018.^[38] In this work, the authors grew SbSI on mesoporous TiO_2 by a three-step process involving the chemical bath deposition of Sb_2S_3 followed by spin-coating of SbI_3 and thermal annealing to react the chalcogenide and halide antimony salts into the desired SbSI. The use of a mesoporous electron transport layer, aside from maximizing the interface with the light absorber and thus the charge extraction, possibly also has a positive effect in limiting the highly anisotropic growth of SbSI (see Table 1). Several organic hole transport materials were tested in this work and a power conversion efficiency (PCE) of 3.05% was achieved (see Figure 4a), later improved to 3.62% in a subsequent report.^[45] Note that this later work also describes the use of SbSI as interlayer in Sb_2S_3 -based solar cells with optimized charge transfer and a PCE of 6.08%. To increase the efficiency of V-VI-VII solar cells, the same group reported the use of mixed-cation ($Sb_{0.67}Bi_{0.33}$)SI in an adaptation of the former work where the initial Sb_2S_3 layer is reacted with BiI_3 instead of SbI_3 .^[46] As already noted in the 1960s (see Table 1) Bi-based V-VI-VII generally absorb a larger portion of the solar spectrum due to a narrower bandgap, which is more suitable for single-junction solar cells. Indeed, Nie et al. achieved a

considerably higher short-circuit current (J_{sc}) close to 15 mA cm^{-2} than with SbSI ($J_{sc} = 9 \text{ mA cm}^{-2}$) and an overall higher PCE of 4.07% (Figure 4b). A complete replacement of Sb by Bi in V-VI-VII materials reduces the bandgap even further, in the range of 1.3–1.6 eV.^[13,14,47–49] This was used by Tiwari et al.^[50] to fabricate BiSI-based solar cells. While the reported efficiency of 1.3% (Figure 4c) is lower than in previous reports by Nie et al.^[38,46] employing SbSI, it is worth noting that in this work the authors employ a planar architecture with BiSI layers grown by a single molecular precursor on top of SnO_2 . The highly irregular morphology consisting of flake-shaped grains or crystallographic domains is probably a major hurdle to the overall photovoltaic performances. Hence, if the morphology of V-VI-VII thin films can be improved during deposition or via different post-deposition treatments, we could expect a further improvement in PV efficiency.

Eventually, it is also interesting to note that bismuth chalcogenides have been employed in related fields such as photoelectrochemical cells^[51] and ionizing radiation detectors.^[52]

4. Mixed-Metal Chalcogenides

Mixed-metal chalcogenide semiconductors have also been reported and investigated for PV. These are usually formed by the combination of a heavy pnictogen (Bi or Sb) and a transition metal cation with a chalcogenide and a halide anion. One example is the silver bismuth sulfiodides $Ag_3BiI_{6-2x}S_x$ which can be seen as a derivative of the mixed-metal halide Ag_3BiI_6 by partial halide-for-chalcogenide anion-exchange. Pai et al.^[53] proposed a one-step spin-coating approach (see Figure 5a) where small amounts of bismuth tris(4-methylbenzodithioate) was added as a sulfur source together with AgI and BiI_3 . After thermal annealing, the corresponding $Ag_3BiI_{6-2x}S_x$ thin films are formed. It must be noted that XPS characterization of the thin films also shows signs of metallic Bi(0) (Figure 5b). This is reminiscent of metallic lead found in lead halide perovskites,^[54] and could undermine the photovoltaic properties by acting as nonradiative recombination centers. Notwithstanding this last observation, as the molar fraction of sulfur (x) is varied from

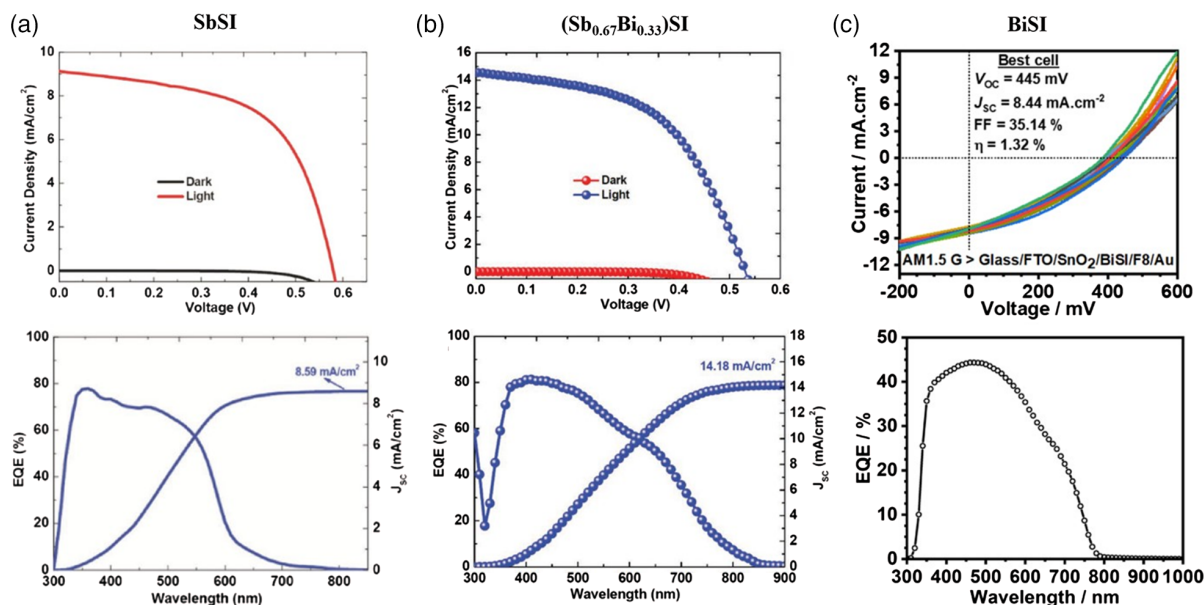


Figure 4. Photovoltaic results (current density–voltage curves and external quantum efficiency–EQE– and integrated short-circuit current) reported with V-VI-VII absorbers. a) Results obtained by Nie et al.^[38] with SbSI. b) Results obtained by the same group with mixed antimony-bismuth sulfide.^[46] c) Results obtained by Tiwari et al.^[50] with BiSI. (a,b) are based on a mesoporous architecture, while (c) uses a planar configuration. The red-shift in bandgap with introduction of Bi (as replacement of Sb) can be observed by the EQE onset shift. This translates into a higher short-circuit current with similar architecture (a,b). Adapted with permission.^[38] Copyright 2018, Wiley. Adapted with permission.^[46] Copyright 2019, Wiley. Adapted with permission.^[50] Copyright 2019, American Chemical Society.

0 to 6% a progressive bandgap narrowing is observed from 1.87 to 1.76 eV (Figure 5c). This results in generally higher short-circuit current (Figure 5d) due to the higher external quantum efficiency (Figure 5e) at longer wavelengths. Nevertheless, fill-factor (FF) and especially open-circuit voltage (V_{oc}) are decreased with the lower-bandgap sulfur-containing materials so that an optimal loading of 4% is found with a power conversion efficiency of 5.4%.

Aside from this silver-bismuth chalcogenide that can arguably be referred to as a sulfur-doped metal halide rather than a true chalcogenide material, there exists a number of reported copper-bismuth chalcogenides including $Cu_3Bi_2S_3I_3$,^[55] $CuBi_2Se_3I$,^[56] and $Cu_3Bi_6S_{10}I$.^[56] These have been experimentally synthesized and characterized. Optical absorption measurements reveal bandgaps of ≈ 0.7 eV. This may seem excessively low for PV at first, but the present record in efficiency for a multijunction solar cell combines absorbers with bandgaps down to 0.69 eV.^[3] Other copper bismuth chalcogenides have been reported with complex compositions and mixed valency elements.^[57,58]

Similarly, Cd,^[59,60] In,^[60] and Hg^[61] quaternary pnictogen chalcogenides have been investigated, but seem unlikely to be implemented today as alternative PV absorbers due to the scarcity and/or toxicity of these elements. Lead-based compounds, despite lead toxicity, have been employed. In particular, Nie et al. reported the use of $Pb_2SbS_2I_3$ in a single-junction solar cell (Figure 6a–d).^[62] To do so, a first layer of Sb_2S_3 was grown by chemical bath deposition on mesoporous TiO_2 . Then, PbI_2 dissolved in DMF was spin coated on top followed by thermal annealing. These last two steps were repeated several times to achieve full conversion of the Sb_2S_3

layer into the desired $Pb_2SbS_2I_3$, as verified by X-ray diffraction (Figure 6a). This film was found to possess a bandgap of 2.19 eV (Figure 6b). Single-junction solar cells were fabricated with $Pb_2SbS_2I_3$ on mesoporous TiO_2 leading to a PCE of 3.12% and a V_{oc} exceeding 600 mV (Figure 6c,d). These results, though promising, present several pitfalls, among which: 1) the toxicity of lead, 2) the complex deposition method including prior growth of Sb_2S_3 followed by conversion requiring repeated spin-coating and annealing steps, and 3) the limited light absorption (and hence limited short-circuit current) due to a very wide bandgap.

These shortcomings were overcome by the same group in a subsequent report on the tin analogue $Sn_2SbS_2I_3$.^[63] This material could be synthesized as thin film with good phase purity (Figure 6e) by a simpler one-step spin-coating approach with a mixture of $SbCl_3$, SnI_2 , and thiourea as sulfur precursor dissolved in DMF. The resulting bandgap of 1.41 eV (Figure 6f) is much narrower than that of the lead analogue, and better suited for photovoltaics. As a result, the short-circuit current increases significantly to 16 mA cm^{-2} (Figure 6g,h) to reach a PCE of 4.04%. Still, open circuit voltage and fill factor remain relatively low (Figure 6g).

Furthermore, bismuth analogues $Sn_2BiS_2I_3$ and Sn_2BiSI_5 , with experimentally determined direct bandgaps of 1.22 and 1.32 eV could also be employed and be optimal for single-junction solar cells.^[64]

Eventually, it is important to mention that mixed-metal chalcogenides are not all pnictogen-based. Indeed, different

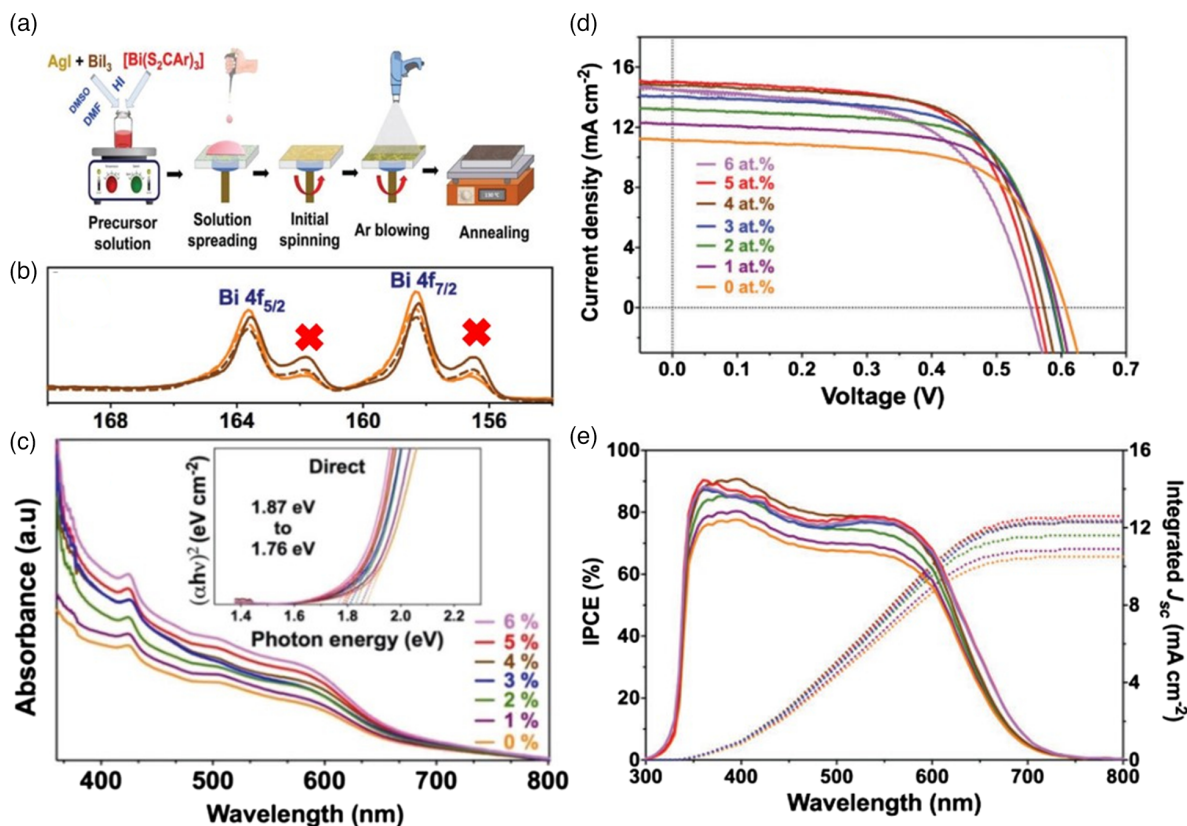


Figure 5. a) Schematic representation of $\text{Ag}_3\text{Bi}_{1-2x}\text{S}_x$ thin film formation. b) XPS Bi 4f spectra of the thin films. Red crosses (not present in original figure) indicate the presence of metallic bismuth. c) UV-vis absorption spectra and Tauc plot inset of films with different loadings of sulfur. d) Current density–voltage curves and e) incident photon to current conversion efficiency as well as integrated short-circuit current of $\text{Ag}_3\text{Bi}_{1-2x}\text{S}_x$ -based solar cells (x values ranging from 0% to 6% given in the legend). Adapted with permission.^[53] Copyright 2019, Wiley.

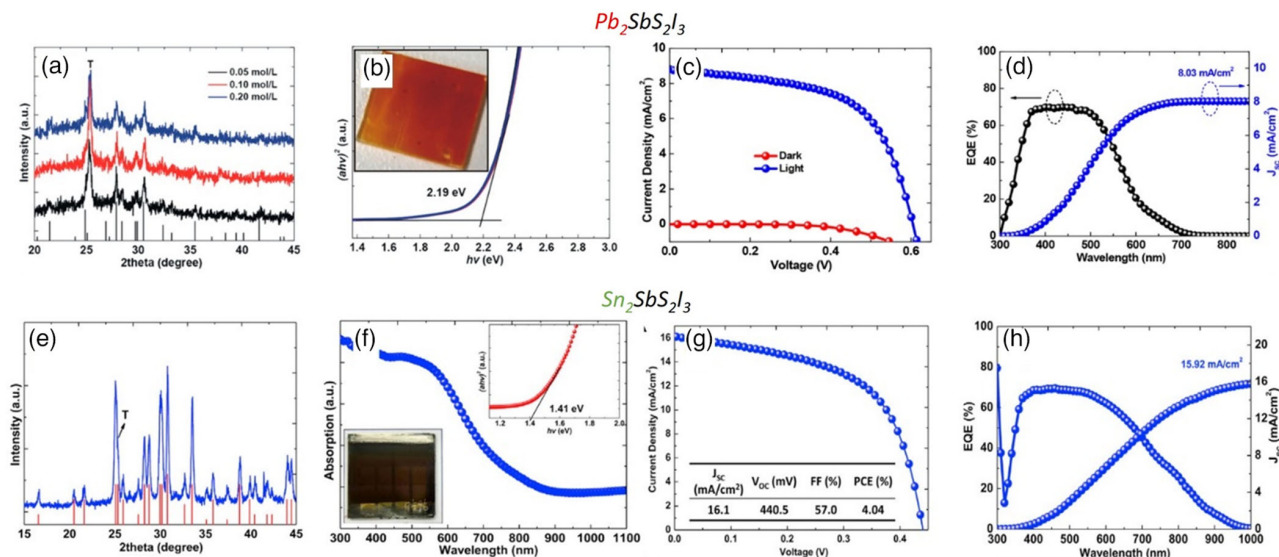


Figure 6. X-ray diffraction (a,e), absorption spectra and Tauc plots with photography insets (b,f), current density–voltage curves (c,g), and external quantum efficiency and integrated short-circuit current (d,h) of $\text{Pb}_2\text{SbS}_2\text{I}_3$ (a–d) and $\text{Sn}_2\text{SbS}_2\text{I}_3$ (e–h) thin films and solar cells. Adapted with permission.^[62] Copyright 2018, American Chemical Society. Adapted with permission.^[63] Copyright 2020, Elsevier.

mercury-based mixed-metal chalcogenides have been reported with bandgaps in the visible range, such as $\text{ZnHg}_3\text{Se}_2\text{Cl}_4$ with a bandgap of 2.23 eV^[65] and $\text{Hg}_7\text{InS}_6\text{Cl}_5$ with a bandgap of 2.54 eV.^[66]

5. Hybrid Organic-Inorganic Metal Chalcogenides?

In a clear analogy with halide perovskites and so-called “vacancy-ordered perovskites”,^[67] some hybrid organic-inorganic metal chalcogenides have been proposed with methylammonium (MA) as monovalent small molecule cation. Vigneshwaran et al.^[68] and Li et al.^[69] synthesized $\text{MA}_3\text{Bi}_2\text{I}_9$ as well as sulfur-doped analogues $\text{MA}_3\text{Bi}_2(\text{S}_x\text{I}_{9-2x})$ obtaining a change in bandgap upon sulfur addition and achieving a PCE of 0.15%. These, however, may be considered more as chalcogenide-doped metal halides rather than chalcogenides, similar to previously discussed reports on silver-bismuth materials.^[53] In 2018, Nie et al.^[70] reported the synthesis and implementation in solar cells of MASbSI_2 . Nevertheless, the existence of this material was later disputed by Li et al.^[71] Therefore, to date, there is no unambiguous report of hybrid organic-inorganic metal chalcogenide semiconductors.

6. Conclusion

As we have seen in the previous sections, metal chalcogenide semiconductors represent a vast family of materials with different compositions, stoichiometries, and optoelectronic properties. Many of these can be considered relevant for photovoltaics, based on different criteria such as bandgap energy and charge carrier

mobility as well as low-toxicity compositions. The degree of investigation of these mostly overlooked materials is also variable, with some materials having been already implemented in solar cells with different architectures and others being only theoretically described. These aspects are summarized in Table 2.

Figure 7 provides a direct visualization of the potential use of different chalcogenides for single-junction (Figure 7a) and two-terminal tandem (Figure 7b) solar cells.

As shown in Table 2 and Figure 7, the wide variety of compositions in metal chalcogenides translates into a wide range of bandgap energies that are relevant for photovoltaics. As such, the best-suited candidates for single-junction devices (Figure 7a) appear to be Sn–Bi–S–I compounds with different stoichiometries, which on top of their ideal bandgap are composed of relatively low-toxicity elements. In fact, $\text{Sn}_2\text{BiS}_2\text{I}_3$ has already been implemented in solar cells as described in Section 4 with a PCE of 4.04%,^[63] which is among the highest reported to date on all metal chalcogenide semiconductors. If we look at either side of these compounds in Figure 7a, we find both low-bandgap and wide-bandgap alternatives, that may be especially relevant for tandem devices (Figure 7b). It must be noted though that, so far, only the wide-bandgap metal chalcogenides have been implemented in (single-junction) solar cells.^[31,45,46,50,53,62] These could potentially be combined with well-established silicon solar cells in high-efficiency tandem devices. Furthermore, Figure 7b reveals that all-chalcogenide tandem cells could in principle reach very high efficiencies as well (e.g., $\text{Pb}_4\text{S}_3\text{I}_2/\text{Ag}_3\text{SI}$ combination could yield over 45% maximum theoretical power conversion efficiency). For this, implementation of low-bandgap chalcogenide absorbers

Table 2. Summary of reported metal chalcogenide semiconductors, bandgap energy, and power conversion efficiency of solar cells employing these materials as light-absorbers. The bandgap energy value is derived from experimental data when available.

Type	Composition	Experimental report	Bandgap	PCE
V–VI–VII	SbSI	Yes	2.15 eV ^[38]	3.62% ^[45] (mesoporous)
	BiSI	Yes	1.57 eV ^[50]	1.32% ^[50] (planar)
	$(\text{Sb}_{0.67}\text{Bi}_{0.33})\text{SI}$	Yes	1.62 eV ^[46]	4.07% ^[46] (mesoporous)
Transition and post-transition metal chalcogenides	Ag_3SI	Yes	0.9–1.1 eV ^[20,21]	—
	Ag_3SBr	Yes	?	—
	$\text{Sn}_5\text{S}_4\text{Cl}_2$	No	0.91 eV ^[30] (theoretical)	—
	$\text{Cd}_5\text{S}_4\text{Cl}_2$	No	2.75 eV ^[30] (theoretical)	—
	Sn_4SF_6	No	3.36 eV ^[30] (theoretical)	—
	Cd_4SF_6	No	2.15 eV ^[30] (theoretical)	—
	$\text{Pb}_3\text{S}_2\text{Cl}_2$	Yes (nanocrystals)	2.02 eV ^[31]	—
	$\text{Pb}_4\text{S}_3\text{Br}_2$	Yes (nanocrystals)	1.98 eV	0.2% ^[31]
$\text{Pb}_4\text{S}_3\text{I}_2$	Yes (nanocrystals)	1.76 eV ^[31]	—	
Mixed-metal chalcogenides	$\text{Ag}_3\text{BiI}_{6-2x}\text{S}_x$	Yes	1.76–1.87 eV	5.5% ^[53]
	$\text{Cu}_3\text{Bi}_2\text{S}_3\text{I}_3$	Yes	? (black) ^[55]	—
	$\text{CuBi}_2\text{Se}_3\text{I}$ and $\text{Cu}_3\text{Bi}_6\text{S}_{10}\text{I}$	Yes	0.7 eV ^[56]	—
	$\text{Pb}_2\text{SbS}_2\text{I}_3$	Yes	2.19 eV	3.12% ^[62] (mesoporous)
	$\text{Sn}_2\text{BiS}_2\text{I}_3$	Yes	1.22 ^[64] –1.41 ^[63] eV	4.04% ^[63] (mesoporous)
	Sn_2BiSI_5	Yes	1.32 eV ^[64]	—

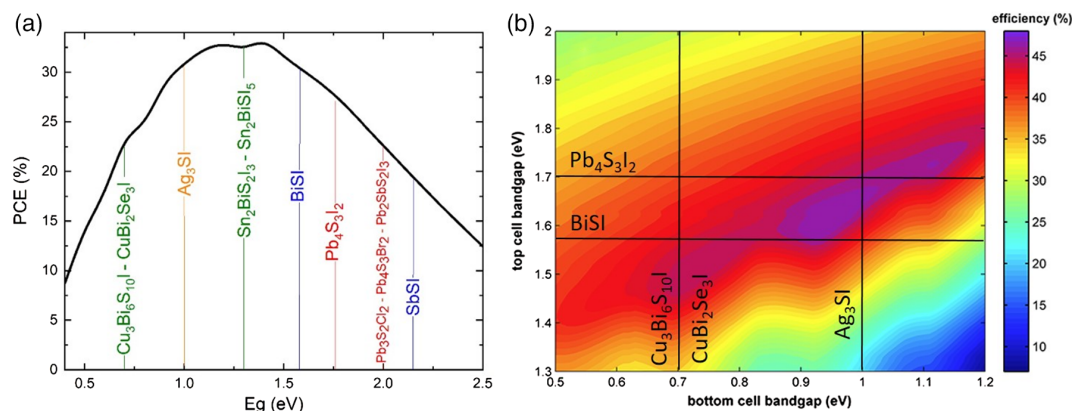


Figure 7. Theoretical maximum PCE achievable with different metal chalcogenides in single-junction (a) and two-terminal tandem (b) solar cells. a) Representation of maximum theoretical PCE under AM 1.5G as a function of bandgap energy (Eg). Different chalcogenides are placed according to reported Eg values (see Table 2). For clarity, different compositions are colored by similarity, that is, low toxicity mixed-metal chalcogenides in green; silver chalcogenide antiperovskites in orange; V–VI–VII compounds in blue; and lead-based (ternary and quaternary) chalcogenides in red. b) Theoretical maximum efficiency of a 2T tandem photovoltaic device. Different low-bandgap and wide-bandgap metal chalcogenides are indicated with vertical and horizontal lines according to their bandgap energy (see Table 2). Adapted with permission.^[74] Copyright 2019, Arizona State University.

in solar cells remains to be demonstrated. One of the major bottlenecks for the further development of metal chalcogenide absorbers resides in the complex synthesis and/or thin-film deposition conditions of these materials. Indeed, as we have previously discussed, some of these such as Ag_3SI antiperovskites typically require very high temperatures and long synthesis times,^[22,23] whereas others such as lead chalcogenides may only be stable in bulk form at high pressure.^[31] Hence, beyond spin-coating of molecular precursors dissolved in organic solvents and mild annealing on a hot plate (methodology largely employed for perovskite PV), novel or unconventional synthesis and deposition approaches should be considered such as mechanochemical synthesis,^[72] pulsed laser deposition,^[73] and/or colloidal synthesis.^[31]

Acknowledgements

The Spanish Ministry of Science is acknowledged for funding: grant IJC2018-036753-I funded by MCIN/AEI/10.13039/501100011033.

Conflict of Interest

The author declare no conflict of interest.

Keywords

bandgaps, chalcogenides, materials, optoelectronics, photovoltaics

Received: October 6, 2021

Revised: November 17, 2021

Published online: December 8, 2021

[1] NREL, *Best Research-Cell Efficiency Chart*, <https://www.nrel.gov/pv/cell-efficiency.html> (accessed: November 2021).

[2] W. Shockley, H. J. Queisser, *J. Appl. Phys.* **1961**, 32, 510.

- [3] J. F. Geisz, R. M. France, K. L. Schulte, M. A. Steiner, A. G. Norman, H. L. Guthrey, M. R. Young, T. Song, T. Moriarty, *Nat. Energy* **2020**, 5, 326.
- [4] F. M. van der Staaij, I. M. van Keulen, E. von Hauff, *Sol. RRL* **2021**, 5, 1.
- [5] J. S. Manser, M. I. Saidaminov, J. A. Christians, O. M. Bakr, P. V. Kamat, *Acc. Chem. Res.* **2016**, 49, 330.
- [6] S. K. Wallace, D. B. Mitzi, A. Walsh, *ACS Energy Lett.* **2017**, 2, 776.
- [7] X. Qiu, B. Cao, S. Yuan, X. Chen, Z. Qiu, Y. Jiang, Q. Ye, H. Wang, H. Zeng, J. Liu, M. G. Kanatzidis, *Sol. Energy Mater. Sol. Cells* **2017**, 159, 227.
- [8] Y. T. Huang, S. R. Kavanagh, D. O. Scanlon, A. Walsh, R. L. Z. Hoyer, *Nanotechnology* **2021**, 32, 132004.
- [9] A. Zakutayev, J. D. Major, X. Hao, A. Walsh, J. Tang, T. K. Todorov, L. H. Wong, E. Saucedo, *J. Phys. Energy* **2021**, 3, 032003.
- [10] E. Wlaźlak, A. Blachecki, M. Biszytyga-Szklarz, S. Klejna, T. Mazur, K. Mech, K. Pilarczyk, D. Przychyna, M. Suchecki, P. Zawal, K. Szaciłowski, *Chem. Commun.* **2018**, 54, 12133.
- [11] Y. C. Choi, K. W. Jung, *Nanomaterials* **2020**, 10, 1.
- [12] L. Gao, J. Huang, S. Guo, Z. Yang, S. Pan, *Coord. Chem. Rev.* **2020**, 421, 213379.
- [13] H. Shi, W. Ming, M. H. Du, *Phys. Rev. B* **2016**, 93, 1.
- [14] Z. Ran, X. Wang, Y. Li, D. Yang, X. G. Zhao, K. Biswas, D. J. Singh, L. Zhang, *npj Comput. Mater.* **2018**, 4, 14.
- [15] B. Reuter, K. Hardel, *Angew. Chem., Int. Ed.* **1960**, 72, 138.
- [16] T. Takahashi, O. Yamamoto, *Electrochim. Acta* **1966**, 11, 779.
- [17] L. Yin, M. Murphy, K. Kim, L. Hu, J. Cabana, D. J. Siegel, S. H. Lapidus, *Inorg. Chem.* **2020**, 59, 11244.
- [18] N. Vicente, G. Garcia-Belmonte, *Adv. Energy Mater.* **2017**, 7, 1.
- [19] P. Calado, A. M. Telford, D. Bryant, X. Li, J. Nelson, B. C. O'Regan, P. R. F. Barnes, *Nat. Commun.* **2016**, 7, 1.
- [20] W. Shimosaka, S. Kashida, M. Kobayashi, *Solid State Ionics* **2005**, 176, 349.
- [21] M. Kurita, K. Nakagawa, F. Akao, *Jpn. J. Appl. Phys.* **1988**, 27, L1920.
- [22] R. B. Beeken, T. J. Wright, T. Sakuma, *J. Appl. Phys.* **1999**, 85, 7635.
- [23] R. B. Beeken, E. M. Beeken, *Solid State Ionics* **2000**, 136–137, 463.
- [24] Y. S. Tver'yanovich, M. D. Bal'makov, V. V. Tomaev, E. N. Borisov, O. Volobueva, *Glas. Phys. Chem.* **2008**, 34, 150.

- [25] R. B. Beeken, E. M. Beeken, *Solid State Ionics* **2000**, 136–137, 463.
- [26] R. B. Beeken, T. J. Wright, T. Sakuma, *J. Appl. Phys.* **1999**, 85, 7635.
- [27] R. B. Beeken, W. L. Jetzer, D. R. Smith, *Solid State Ionics* **1994**, 70/71, 176.
- [28] R. B. Beeken, K. L. Menningen, *J. Appl. Phys.* **1989**, 66, 5340.
- [29] J. Kawamura, M. Siitmoji, H. Hoshino, *J. Phys. Soc. Jpn.* **1981**, 50, 194.
- [30] D. W. Davies, K. T. Butler, J. M. Skelton, C. Xie, A. R. Oganov, A. Walsh, *Chem. Sci.* **2018**, 9, 1022.
- [31] S. Toso, Q. A. Akkerman, B. Martín-García, M. Prato, J. Zito, I. Infante, Z. Dang, A. Moliterni, C. Giannini, E. Bladt, I. Lobato, J. Ramade, S. Bals, J. Buha, D. Spirito, E. Mugnaioli, M. Gemmi, L. Manna, *J. Am. Chem. Soc.* **2020**, 142, 10198.
- [32] S. Johnsen, Z. Liu, J. A. Peters, J. H. Song, S. Nguyen, C. D. Malliakas, H. Jin, A. J. Freeman, B. W. Wessels, M. G. Kanatzidis, *J. Am. Chem. Soc.* **2011**, 133, 10030.
- [33] Q. A. Akkerman, G. Rainò, M. V. Kovalenko, L. Manna, *Nat. Mater.* **2018**, 1.
- [34] G. Henry, *J. Pharm.* **1824**, 10, 511.
- [35] R. Nitsche, W. J. Merz, *J. Phys. Chem. Solids* **1960**, 13, 154.
- [36] E. Fatuzzo, G. Harbeke, W. J. Merz, R. Nitsche, H. Roetschi, W. Ruppel, *Phys. Rev.* **1962**, 127, 2036.
- [37] K. T. Butler, S. McKechnie, P. Azarhoosh, M. Van Schilfgaarde, D. O. Scanlon, A. Walsh, *Appl. Phys. Lett.* **2016**, 108, 112103.
- [38] R. Nie, H. S. Yun, M. J. Paik, A. Mehta, B. W. Park, Y. C. Choi, S. Il Seok, *Adv. Energy Mater.* **2018**, 8, 1.
- [39] R. Kern, *J. Phys. Chem. Solids* **1962**, 23, 249.
- [40] S. Surthi, S. Kotru, R. K. Pandey, *Integr. Ferroelectr.* **2002**, 48, 263.
- [41] G. Chen, W. Li, Y. Yu, Q. Yang, *RSC Adv.* **2015**, 5, 21859.
- [42] M. Tasviri, Z. Sajadi-Hezave, *Mol. Catal.* **2017**, 436, 174.
- [43] K. T. Butler, J. M. Frost, A. Walsh, *Energy Environ. Sci.* **2015**, 8, 838.
- [44] A. M. Ganose, C. N. Savory, D. O. Scanlon, *Chem. Commun.* **2017**, 53, 20.
- [45] R. Nie, S. Il Seok, *Small Methods* **2020**, 4, 1.
- [46] R. Nie, J. Im, S. Il Seok, *Adv. Mater.* **2019**, 31, 1.
- [47] A. Audzijonis, R. Altauskas, R. Sereika, L. Igas, A. Rza, *J. Phys. Chem. Solids* **2010**, 71, 884.
- [48] H. Kunioku, M. Higashi, R. Abe, *Sci. Rep.* **2016**, 6, 1.
- [49] A. M. Ganose, S. Matsumoto, J. Buckeridge, D. O. Scanlon, *Chem. Mater.* **2018**, 30, 3827.
- [50] D. Tiwari, F. Cardoso-Delgado, D. Alibhai, M. Mombrú, D. J. Fermin, *ACS Appl. Energy Mater.* **2019**, 2, 3878.
- [51] C. Zhou, R. Wang, C. Jiang, J. Chen, G. Wang, *Ind. Eng. Chem. Res.* **2019**, 58, 7844.
- [52] M. M. Frutos, M. E. P. Barthaburu, L. Fornaro, I. Aguiar, *Nanotechnology* **2020**, 31, 225710.
- [53] N. Pai, J. Lu, T. R. Gengenbach, A. Seeber, A. S. R. R. Chesman, L. Jiang, D. C. Senevirathna, P. C. Andrews, U. Bach, Y. B. Cheng, A. N. Simonov, *Adv. Energy Mater.* **2018**, 9, 1.
- [54] G. Sadoughi, D. E. Starr, E. Handick, S. D. Stranks, M. Gorgoi, R. G. Wilks, M. Bär, H. J. Snaith, *ACS Appl. Mater. Interfaces* **2015**, 7, 13440.
- [55] T. Balić-Zunić, K. Mariolacos, K. Friese, E. Makovicky, *Acta Crystallogr. Sect. B Struct. Sci.* **2005**, 61, 239.
- [56] I. C. Liang, D. I. Bilc, M. Manoli, W. Y. Chang, W. F. Lin, T. Kyratsi, K. F. Hsu, *J. Solid State Chem.* **2016**, 234, 1.
- [57] A. Heerwig, C. L. J. Thybaut, M. Ruck, *Z. Anorg. Allg. Chem.* **2010**, 636, 2433.
- [58] A. Heerwig, A. Isaeva, M. Ruck, *Z. Anorg. Allg. Chem.* **2011**, 637, 1131.
- [59] L. Wang, Y. C. Hung, S. J. Hwu, H. J. Koo, M. H. Whangbo, *Chem. Mater.* **2006**, 18, 1219.
- [60] L. Wang, S. J. Hwu, *Chem. Mater.* **2007**, 19, 6212.
- [61] A. C. Wibowo, C. D. Malliakas, D. Y. Chung, J. Im, A. J. Freeman, M. G. Kanatzidis, *Inorg. Chem.* **2013**, 52, 2973.
- [62] R. Nie, B. Kim, S. T. Hong, S. Il Seok, *ACS Energy Lett.* **2018**, 3, 2376.
- [63] R. Nie, K. S. Lee, M. Hu, M. J. Paik, S. Il Seok, *Matter* **2020**, 3, 1701.
- [64] S. M. Islam, C. D. Malliakas, D. Sarma, D. C. Maloney, C. C. Stoumpos, O. Y. Kontsevoi, A. J. Freeman, M. G. Kanatzidis, *Chem. Mater.* **2016**, 28, 7332.
- [65] G. Zhang, W. W. Xiong, L. Nie, Q. Zhang, *J. Solid State Chem.* **2015**, 230, 182.
- [66] Y. Liu, F. Wei, S. N. Yeo, F. M. Lee, C. Kloc, Q. Yan, H. H. Hng, J. Ma, Q. Zhang, *Inorg. Chem.* **2012**, 51, 4414.
- [67] Q. A. Akkerman, L. Manna, *ACS Energy Lett.* **2020**, 604.
- [68] M. Vigneshwaran, T. Ohta, S. Iikubo, G. Kafil, T. S. Ripolles, Y. Ogomi, T. Ma, S. S. Pandey, Q. Shen, T. Toyoda, K. Yoshino, T. Minemoto, S. Hayase, *Chem. Mater.* **2016**, 28, 6436.
- [69] J. Li, X. Liu, J. Xu, J. Chen, C. Zhao, M. Salma Maneno, B. Zhang, J. Yao, *Sol. RRL* **2019**, 3, 1.
- [70] R. Nie, A. Mehta, B. W. Park, H. W. Kwon, J. Im, S. Il Seok, *J. Am. Chem. Soc.* **2018**, 140, 872.
- [71] T. Li, X. Wang, Y. Yan, D. B. Mitzi, *J. Phys. Chem. Lett.* **2018**, 9, 3829.
- [72] F. Palazon, Y. El Ajjouri, H. J. Bolink, *Adv. Energy Mater.* **2019**, 1902499, 1.
- [73] N. Rodkey, S. Kaal, P. Sebastia-Luna, Y. A. Birkhölzer, M. Ledinsky, F. Palazon, H. J. Bolink, M. Morales-Masis, *Chem. Mater.* **2021**, 33, 7417.
- [74] C. B. Honsberg, S. G. Bowden, *Photovoltaics Education Website* **2019**, <https://www.pveducation.org> (accessed: November 2021).



Francisco Palazon received his Ph.D. from the Ecole Centrale Lyon in France in 2014. After a post-doctoral contract at the Istituto Italiano di Tecnologia (Italy) from 2015 to 2017, he moved to Spain to develop an independent research career at the Instituto de Ciencia Molecular of the University of Valencia, first with a Marie Skłodowska-Curie Individual Fellowship and later with Juan de la Cierva and Ramón y Cajal contracts (tenure-track position) from the Spanish Ministry of Science. His research is focused on developing novel low-toxicity inorganic semiconductors for photovoltaics and related applications.